Supplementary Information

Mucus-inspired organogel as an efficient absorbent and retention agent for volatile organic compounds

Jihoon Han[a†], Jemin Lee[b†], Seonghyeon Kim[b], Anna Lee[b], Hyung Gyu Park[b*] and Youn Soo Kim[a*]
*To whom correspondence should be addressed
E-mail: ysookim@postech.ac.kr

Table of Contents

1. Materials

N,N-dimethylacrylamide (DMA), 2-acrylamido-2-methylpropane sulfonic acid (AMPS), (3-acrylamidopropyl)trimethylammonium chloride solution (APTC), 2,2′-azobis(2-methylpropionamidine) dihydrochloride (V-50), 4-((((2-carboxyethyl)thio)carbonothioyl)thio)-4-cyanopentanoic acid (CETCPA), *N*,*N*′-methylenebisacrylamide (MBAA), sodium nitrate ($NaNO_3$), sodium phosphate monobasic (NaH_2PO_4), sodium phosphate dibasic (Na_2HPO_4), deuterium oxide (D_2O), and dimethyl sulfoxide-d_6 (DMSO-d_6) were purchased from Sigma-Aldrich. Methanol (MeOH), sulfuric acid (H_2SO_4), sodium hydroxide (NaOH), benzene, toluene, *o*-xylene, *m*-xylene, and *p*-xylene were purchased from Samchun Chemical. All the chemicals were used without further purification. AMPS was neutralized by NaOH before polymerization. A VOC sensor (POLI MP400P, MC Masters) was used to measure VOC concentration. Ultrapure water with a resistivity of 18.2 MΩcm (Direct-Q® 5UV; Merck Millipore) was utilized in all the experiments.

2. Polymer structure

The total degree of polymerization (DP) of the designed DMA homopolymer was 750. The total DP of the designed triblock copolymer was 1050. Two ionic blocks with DP = 150 were located at the ends of the polymer chain, and a neutral DMA block with DP = 750 was in the middle.

Synthesis of multiblock copolymers by RAFT polymerization

Synthesis of neutral poly(DMA). Phosphate buffer solution (16 mL, 10 mM, pH = 7), 4-((((2-carboxyethyl)thio)carbonothioyl)thio)-4-cyanopentanoic acid (CETCPA) (17.9 mg, 3.82 mM), DMA (4,125 mg, 2.70 M), and 2,2′-azobis(2-methylpropionamidine) dihydrochloride (V-50) (1.0 mg, 0.24 mM) were added to a 100 mL glass flask equipped with a magnetic stirrer and sealed with a rubber septum to synthesize poly(DMA). The mixture was deoxygenated by freeze–pump–thaw cycling over three times, followed by polymerization at 70 °C using a temperature-controlled heating mantle and subsequent stirring at 60 rpm for 2 h to reach nearly full conversion. A sample was extracted from the polymerization medium using a degassed syringe for ^{1}H NMR and GPC analyses to determine the monomer conversion, $M_{n,GPC}$, and $Đ$ values.

Synthesis of neutral poly(DMA) gel. Phosphate buffer solution (16 mL, 10 mM, pH = 7), 4-((((2-carboxyethyl)thio)carbonothioyl)thio)-4-cyanopentanoic acid (CETCPA) (17.9 mg, 3.82 mM), DMA (4,125 mg, 2.70 M), 2,2′-azobis(2-methylpropionamidine) dihydrochloride (V-50) (1.0 mg, 0.24 mM), and *N*,*N*′-methylenebisacrylamide (MBAA) (2 mg, 0.65 mM) were added to a 100 mL glass flask equipped with a magnetic stirrer and sealed with a rubber septum to synthesize poly(DMA). The mixture was deoxygenated by freeze–pump–thaw cycling over three times followed by polymerization at 70 °C using a temperature-controlled heating mantle and subsequent stirring at 60 rpm for 2 h to reach nearly full conversion. A sample was extracted from the polymerization medium using a degassed syringe for ^{1}H NMR and GPC analyses to determine the monomer conversion, $M_{n,GPC}$, and $Đ$ values.

Synthesis of anionic poly(AMPS). Phosphate buffer solution (6 mL, 10 mM, pH = 7), 4-((((2-carboxyethyl)thio)carbonothioyl)thio)-4-cyanopentanoic acid (CETCPA) (17.9 mg, 6.09 mM), AMPS (1,725 mg, 0.87 M), and 2,2′-azobis(2-methylpropionamidine) dihydrochloride (V-50) (2.0 mg, 0.77 mM) were added to a 100 mL glass flask equipped with a magnetic stirrer and sealed with a rubber septum to synthesize poly(AMPS). The mixture was deoxygenated by freeze–pump–thaw cycling over three times followed by polymerization at 70 °C using a temperature-controlled heating mantle and subsequent stirring at 60 rpm for 2 h to reach nearly full conversion. A sample was extracted from the polymerization medium using a degassed syringe for ^{1}H NMR and GPC analyses to determine the monomer conversion, $M_{n,GPC}$, and $Đ$ values.

Synthesis of cationic poly(APTC). Phosphate buffer solution (6 mL, 10 mM, pH = 7), 4-((((2-carboxyethyl)thio)carbonothioyl)thio)-4-cyanopentanoic acid (CETCPA) (17.9 mg, 6.58 mM), APTC (1,805 mg, 0.98 M), and 2,2′-azobis(2-methylpropionamidine) dihydrochloride (V-50) (3.5 mg, 1.46 mM) were added to a 100 mL glass flask equipped with a magnetic stirrer and sealed with a rubber septum to synthesize poly(APTC). The mixture was deoxygenated by freeze–pump–thaw cycling over three times followed by polymerization at 70 °C using a temperature-controlled heating mantle and subsequent stirring at 60 rpm for 2 h to reach nearly full conversion. A sample was extracted from the polymerization medium using a degassed syringe for ^{1}H NMR and GPC analyses

to determine the monomer conversion, $M_{n,GPC}$, and $Đ$ values.

Synthesis of subsequent blocks. For the subsequent block extension, the deoxygenated monomer, initiator, and solvent mixture were injected into the polymerization medium. The resultant mixture was polymerized at 70 °C using a temperature-controlled heating mantle followed by stirring at 60 rpm for 2 h to reach nearly full conversion. Before each injection, a sample was extracted from the polymerization medium using a degassed syringe for ^{1}H NMR and GPC analyses to determine the monomer conversion, $M_{n,GPC,}$ and $Đ$ values.

Determination of monomer conversions. For the polymers, monomer conversions were determined using ^{1}H NMR to compare the decrease in the integrated intensity of the vinyl protons (δ = 6.70–5.70 ppm) of the monomer with that of the *R* group protons (δ = 3.60–2.75 ppm) of the monomer and polymer after polymerization.

Preparation of sols and gels. The dialyzed polymers were rapidly frozen in liquid nitrogen and then freeze-dried at a temperature of −50 °C and pressure of 0.1 Pa for 3 days using a freeze dryer (HyperCOOL HC3055, GYROZEN) to obtain a polymer powder. To fabricate the 5,10 and 15 wt% plus and minus sols, the corresponding amount of cationic or anionic triblock polyelectrolyte powder was dissolved in deuterated DMSO. 5, 10, and 15 wt% ionic gels were prepared by mixing 5, 10, and 15 wt% cationic and anionic sols, respectively, with the same volumes. To produce the 10 wt% neutral sol and gel, the corresponding amount of poly(DMA) and poly(DMA) gel powders were dissolved in deuterated DMSO.

3. CFD simulation method

CFD analysis was performed using COMSOL Multiphysics commercial software to simulate benzene concentration monitoring. As the benzene diffusion experiment was conducted in an axisymmetric glass desiccator, the simulation was conducted in 2D-axisymmetric conditions to reduce the cost of analysis. The behavior of benzene molecules inside the chamber was calculated by Fick's law, which is the governing equation regarding the relationship between the particle density

and diffusion rate of molecules.

$$J = -D_b \nabla C_b$$

$$\frac{\partial C_b}{\partial t} + \nabla \cdot J = 0$$

where J and C_b represent the flux and concentration of benzene, respectively. D_b represents the diffusivity of benzene at room temperature and was set to $9.3 \times 10^{-6}\, m^2/s$. Internal air and benzene gas spread by diffusion without convective conditions, assuming that it was completely static. Initially, only air occupied the desiccator, and the liquid benzene at the bottom of the desiccator began to evaporate and diffused into the air. The benzene concentration at the center changed with time, as shown in Fig. S6. The benzene evaporation rate was acquired by measuring the amount of evaporated benzene over 5 min by placing a scale in the desiccator and applying this to the simulation condition. In addition, a mesh independence test was performed on the obtained results to ensure accurate simulation results.

4. GPC studies

Molar mass distributions were measured on a Shimadzu LC-20AD liquid chromatography system using dedicated columns for anionic and cationic polymers. For the anionic polymers, an Agilent PL-aquagel-OH, 8 μm, MIXED-M column (300 × 7.5 mm) and Agilent PL-aquagel-OH, 8 μm, guard column (50 × 7.5 mm) were utilized. The mobile phase consisted of a 90% 0.15 M $NaNO_3$ aqueous solution and 10% methanol. The flow rate was 1.0 mL min^{-1} at a temperature of 40 °C. For the cationic polymers, a TOSOH TSKgel, 10 μm, G5000PWXL-CP column (300 × 7.8 mm) and TOSOH TSKgel, 13 μm, PWXL-CP guard column (40 × 6 mm) were used. The mobile phase consisted of a 0.3 M $NaNO_3$ aqueous solution with pH = 3 attuned by sulfuric acid. The flow rate was 1.0 mL min^{-1} and the temperature was 40 °C. The instrument was calibrated with low-dispersity poly(ethyleneoxide) standards (Scientific Polymer) with varied molar masses between 0.2 and 800 kg mol^{-1}. Analyte samples were filtered through a polyvinylidene fluoride membrane with 0.2-μm pores before injection. The experimental molar mass ($M_{n,GPC}$) and dispersity ($Đ$) values of the synthesized polymers were determined by conventional calibration using LC Solution software with a known RI detector calibration constant.

5. Stokes–Einstein Gierer–Wirtz Estimation (SEGWE) method

The diffusion coefficient of benzene in DMSO was obtained from the SEGWE method.

$$D = \frac{k_B T\left(\frac{3a}{2} + \frac{1}{1+a}\right)}{6\pi\eta\sqrt[3]{\frac{3MW}{4\pi p_{eff} N_A}}},\ \left(a = \frac{r_s}{r} = \sqrt[3]{\frac{MW_s}{MW}}\right)$$

k_B(Boltzmann coefficient): 1.38 × 10^{-23} J/K

T (temperature): 298.15 K

η (dynamic viscosity): 2 × 10^{-3} kg/m·s

MW (molecular mass of benzene): 78.11 g/mol

MW_s (molecular mass of DMSO): 78.13 g/mol

p_{eff} (effective density): 699 kg/m^3

N_A (Avogadro's constant): 6.02 × 10^{23} mol^{-1}

D = 6.17 × 10^{-10} m^2/s

6. Differential scanning calorimetry (DSC)

Thermal transitions of the sols and gels were measured using DSC (Q20, TA Instruments). 1 mg of sol and gel were sealed in an aluminum pan to prevent evaporation of the solvent. First, the sample was cooled to below −80 ℃ at a rate of 10 ℃/min and then heated at the same rate. A thermogram for each sol and gel was obtained in the temperature range of –80 to 30 ℃ at a heating/cooling rate of 10 ℃/min.

7. Avrami model

Methodology

We analyzed the desorption kinetics of VOCs from various matrices in an open system using the Avrami fractional-order kinetic model.[1] The portion corresponding to desorption is the rest except for the amount separated from the absorbent at the initial value.[2] This model has been applied to describe the desorption of VOCs in matrices with different viscosities. The desorption model is as

follows:

$$q = q_e \times e^{-(k_A t)^n} \quad (1)$$

where q is the VOC concentration in the matrix at time t, q_e is the VOC concentration at the initial state, k_A is the Avrami kinetic constant, and n is the Avrami exponent. All the desorption results followed the model best when n = 1, suggesting homogeneous desorption, which means that the probability of desorption is the same for any region during a given time interval.[3] We also assumed that the specific interactions between the VOCs and polymers were negligible. To obtain the model parameters, we fitted the experimental data of VOC concentration in the matrices using OriginPro 2021b.

8. Supplementary Figures 1–22

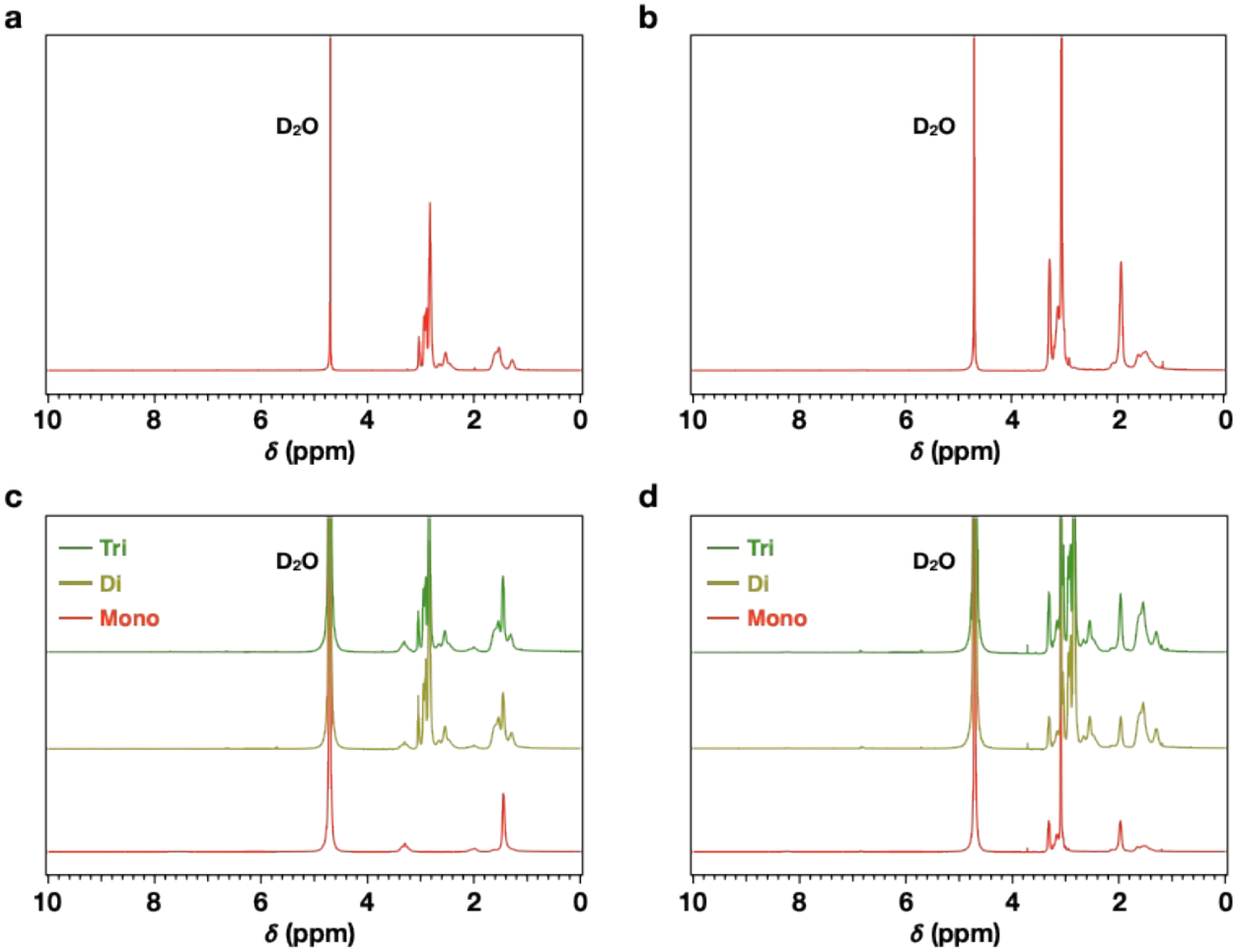

Supplementary Figure 1 | ^{1}H NMR spectra of the (a) neutral polymer, (b) neutral gel, and consecutive block extensions of (c) anionic and (d) cationic triblock polyelectrolytes. The monomer conversion for each spectrum is >99%.

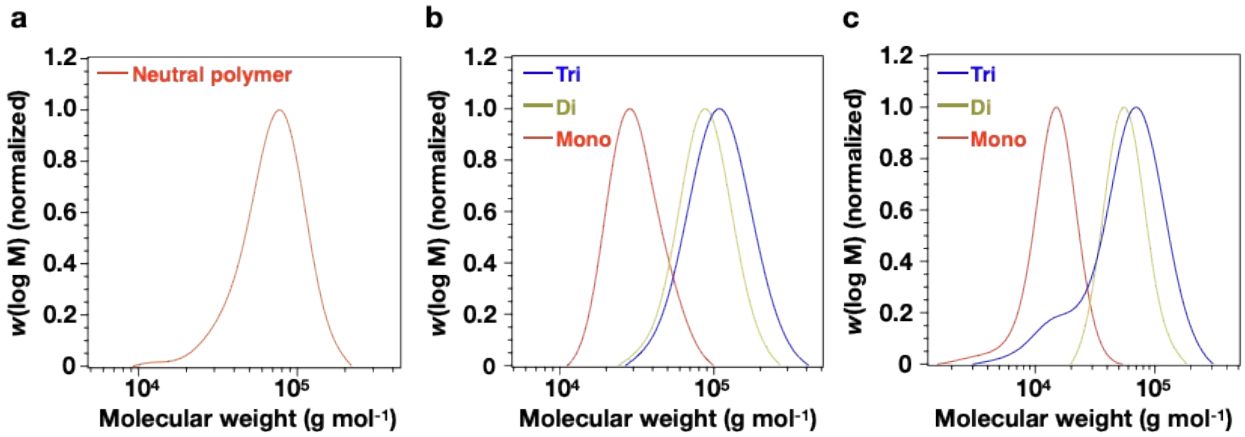

Supplementary Figure 2 | GPC traces of the molecular weight distributions of the (a) neutral polymer and consecutive block extensions of (b) anionic and (c) cationic triblock polyelectrolytes. On the y-axis, *w*(logM) represents the differential logarithmic molecular weight.

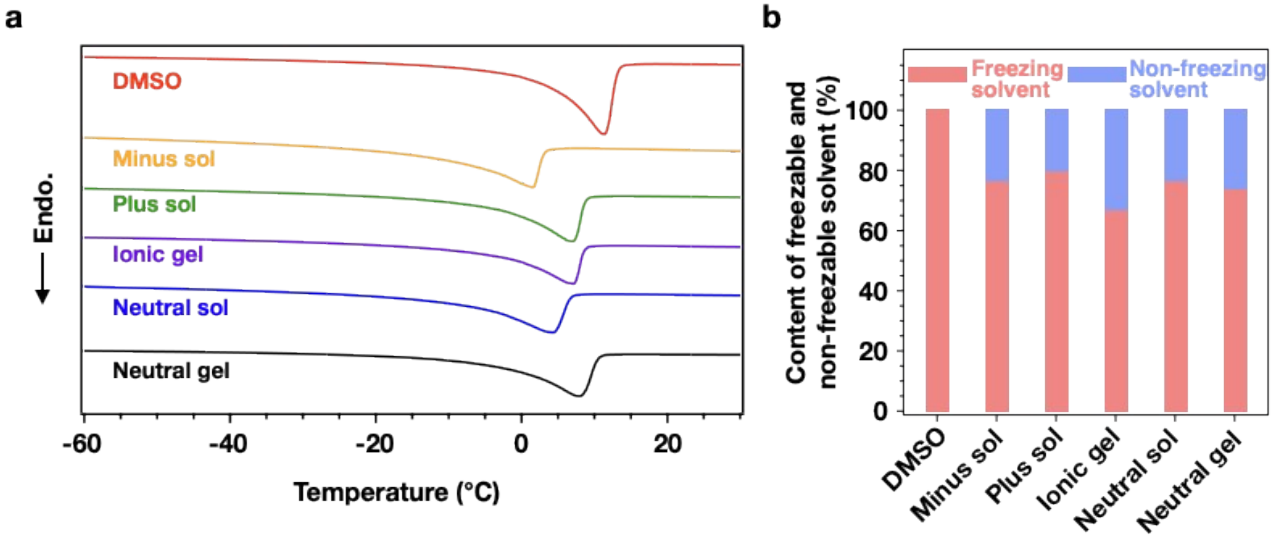

Supplementary Figure 3 | (a) DSC curves of all the matrices for the characterization of freezable DMSO. (b) Ratio of freezable and non-freezable DMSO in all the matrices.

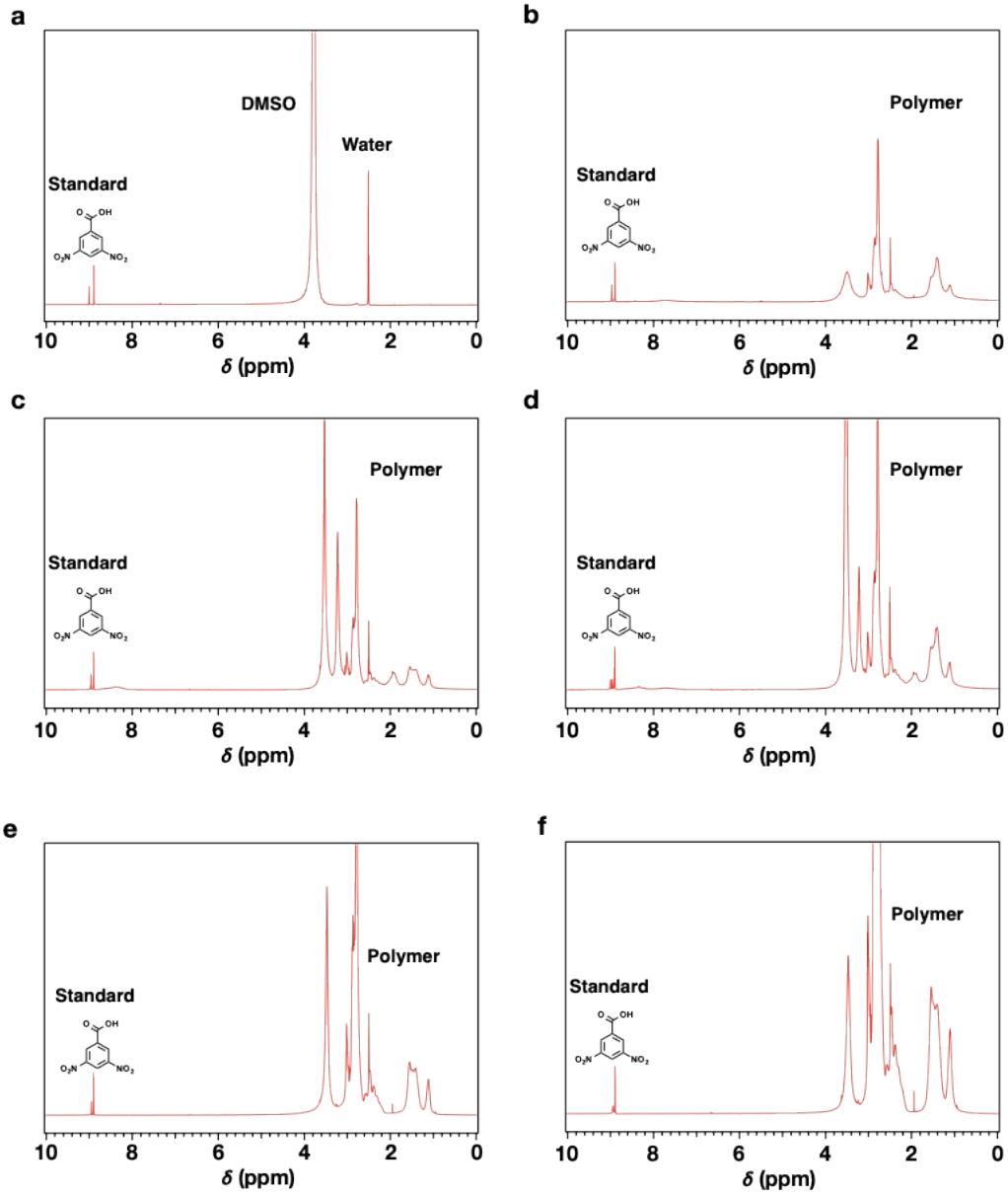

Supplementary Figure 4 | ^{1}H NMR spectra of (a) DMSO, (b) anionic sol, (c) cationic sol, (d) ionic gel, (e) neutral sol, and (f) neutral gel containing standard material.

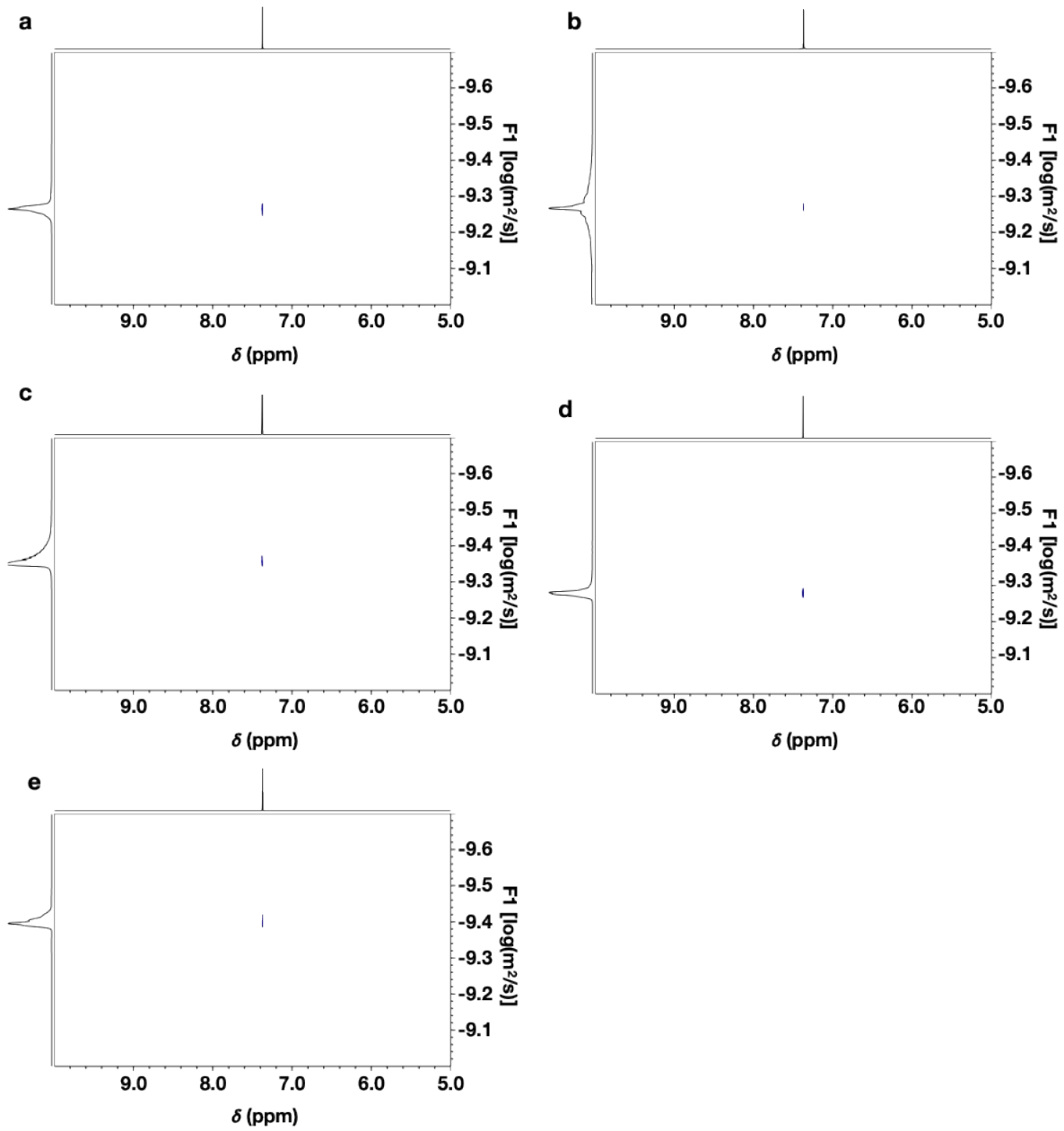

Supplementary Figure 5 | Diffusion coefficient of benzene measured by 2D DOSY experiment in (a) anionic sol, (b) cationic sol, (c) ionic gel, (d) neutral sol, and (e) neutral gel.

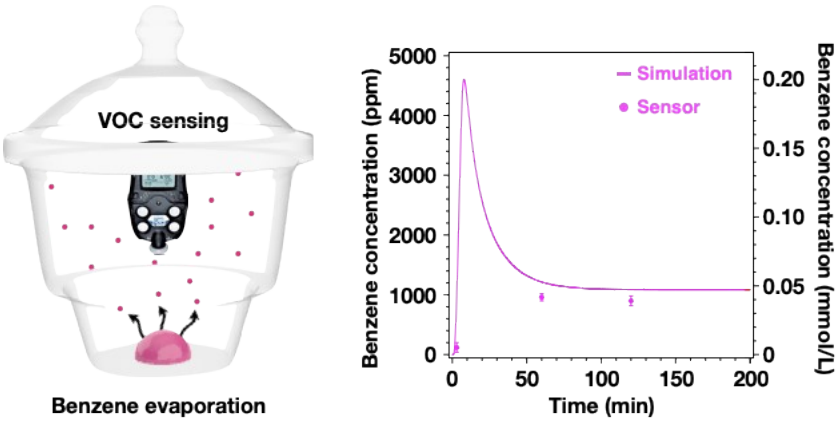

Supplementary Figure 6 | Schematic of simulation conditions and concentration of benzene inside the desiccator as a function of time.

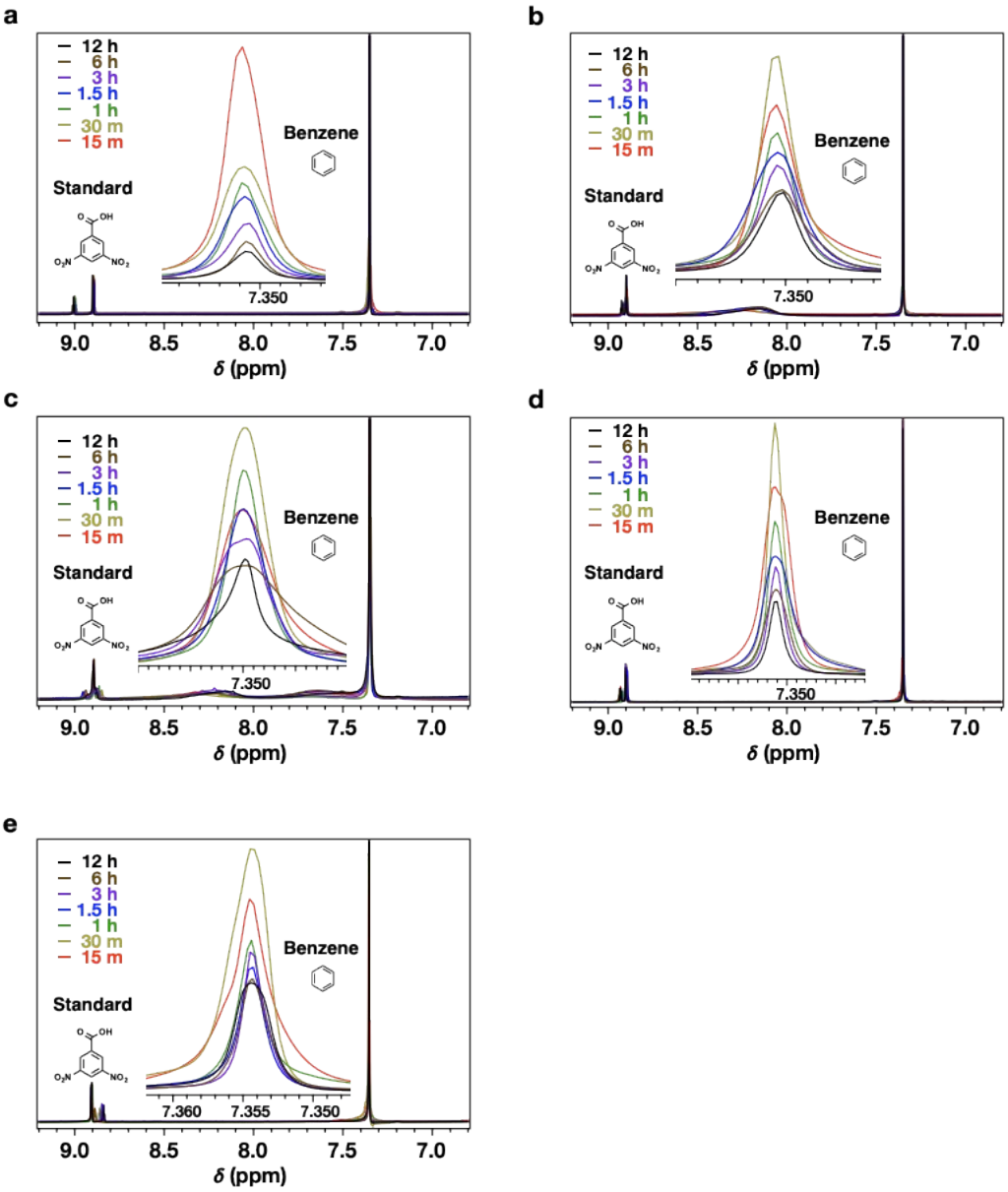

Supplementary Figure 7 | Concentration of benzene in (a) DMSO, (b) cationic sol, (c) ionic gel, (d) neutral sol, and (e) neutral gel over time in a closed system measured by ^{1}H NMR spectroscopy.

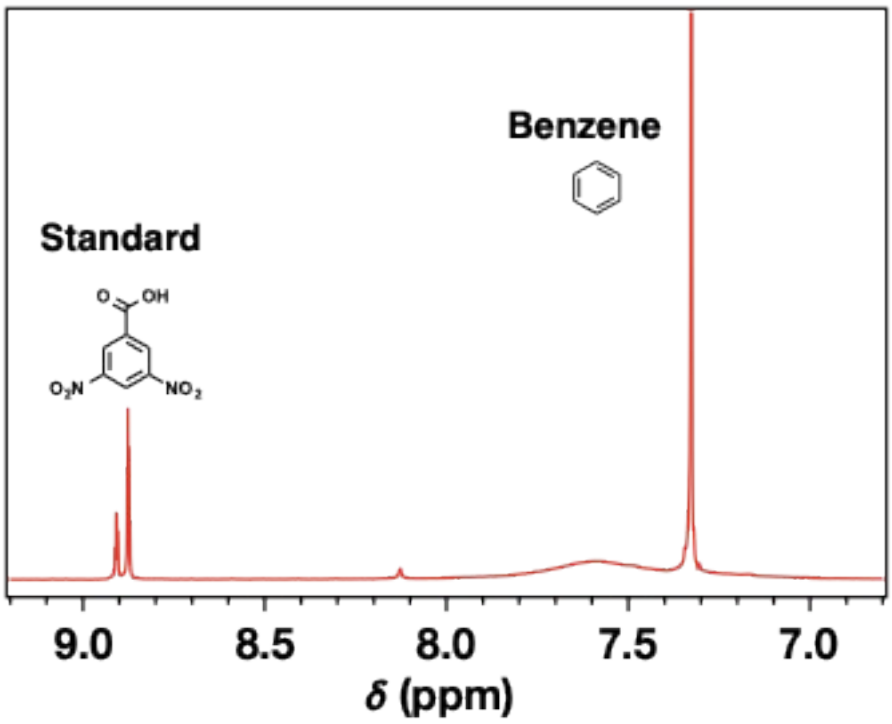

Supplementary Figure 8 | ^{1}H NMR spectrum of an anionic sol containing benzene and standard material. Because the peaks of the anionic polymer and benzene overlap in the ^{1}H NMR spectrum, the experiment was not conducted with the minus sol matrix.

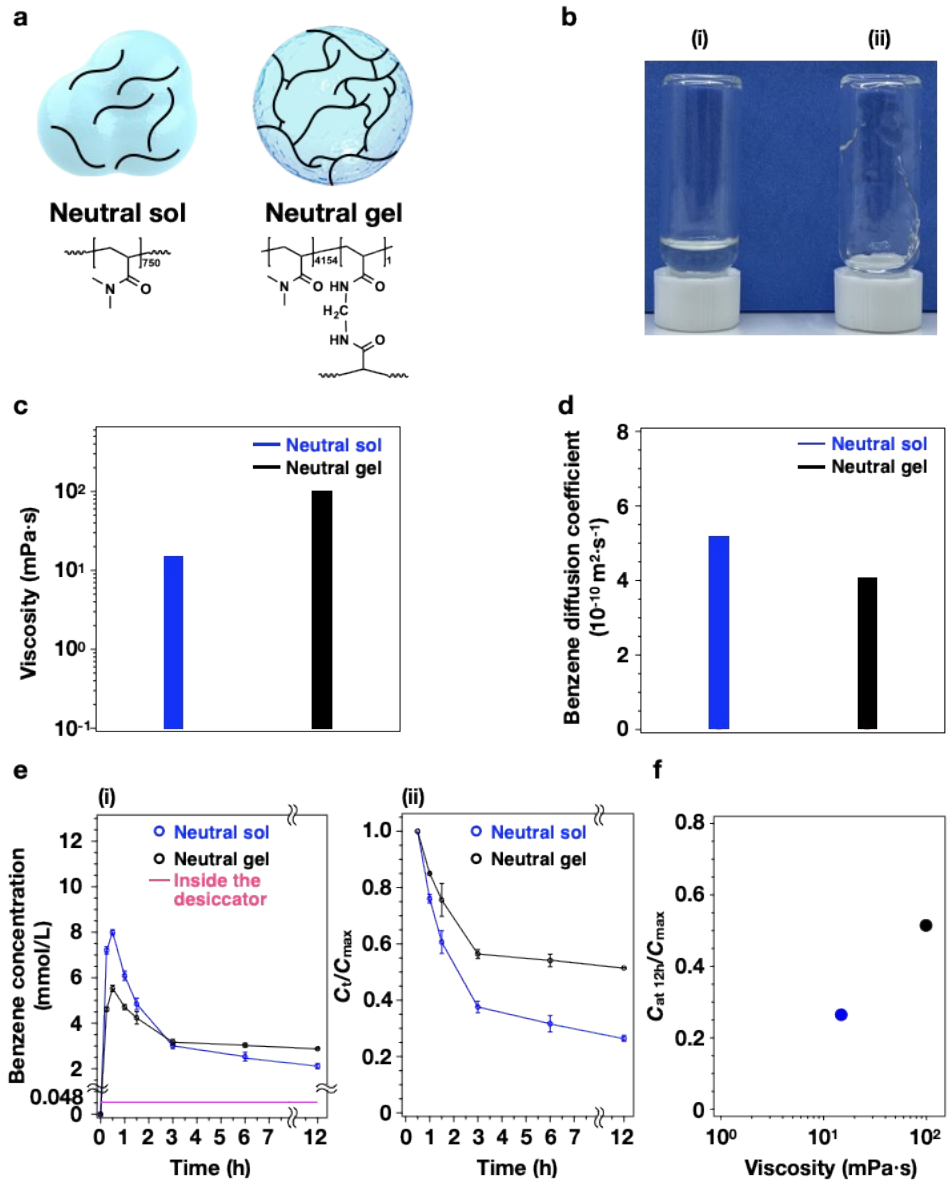

Supplementary Figure 9 | (a) Schematic of the solvent, neutral sol, and gel. (b) Viscosity of the neutral sol and gel. (c) Photographs of inverted vials to compare the viscosities of the neutral sol and gel. (d) Diffusion coefficients of benzene in the matrices. (e) (i) Benzene concentration in the matrices as a function of time. The benzene concentration in the desiccator is 0.048 mmol/L. (ii) Time-dependent change of the benzene concentration at a specific time (C_t) for the C_{max} of each matrix. (f) Benzene retention efficiency as a function of viscosity over the experimental time range.

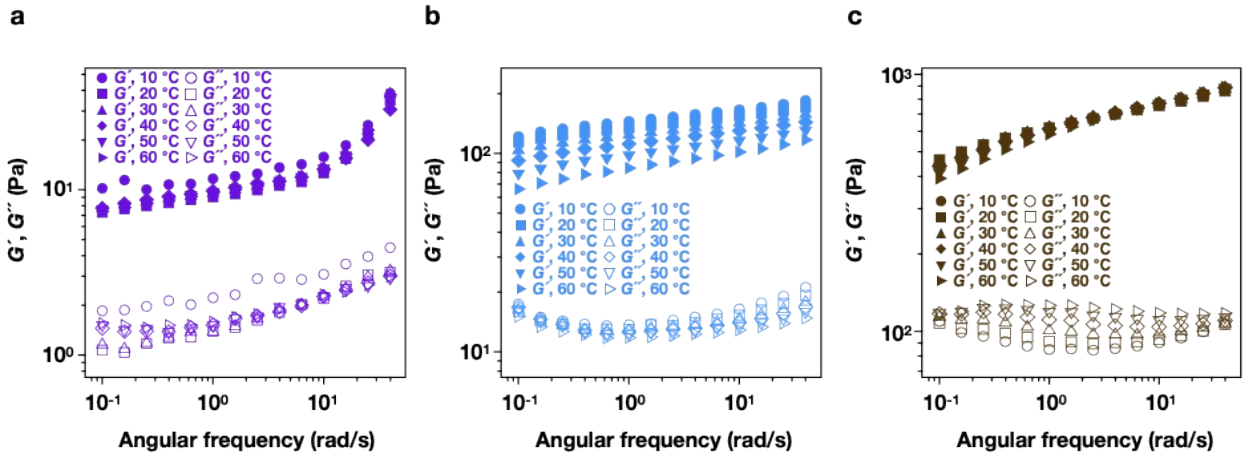

Supplementary Figure 10 | Angular frequency and temperature dependencies of the storage (G') and loss (G'') moduli of the three ionic gels. The frequency sweep was performed from 0.1 to 40 rad s^{-1} at a strain of 1%. Storage (G', closed symbols) and loss (G'', open symbols) moduli of the ionic gels with (a) 5, (b) 10, and (c) 15 wt% polymer concentrations.

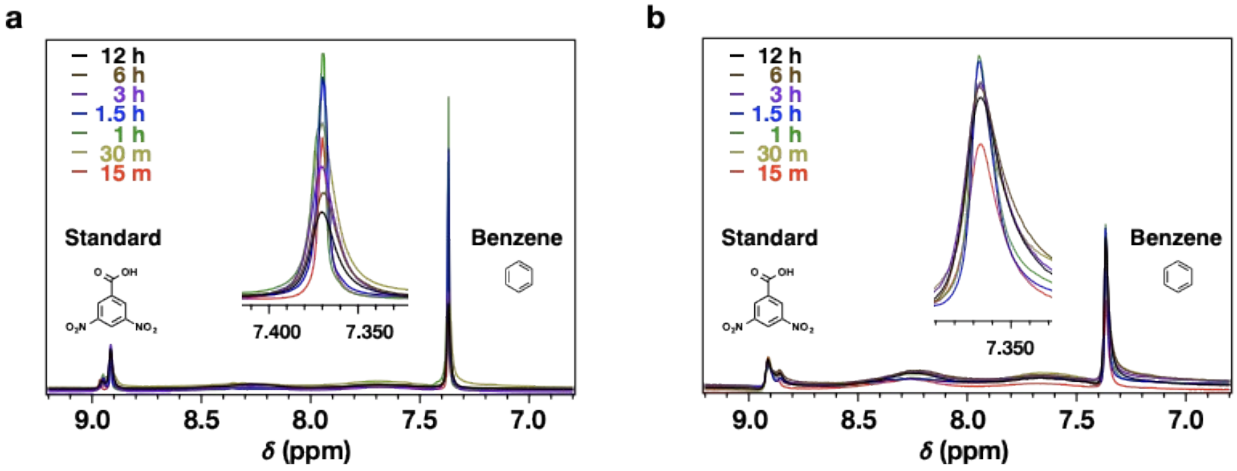

Supplementary Figure 11 | Concentrations of benzene in (a) 10 and (b) 15 wt% ionic gels measured over time in a closed system through ^{1}H NMR spectroscopy.

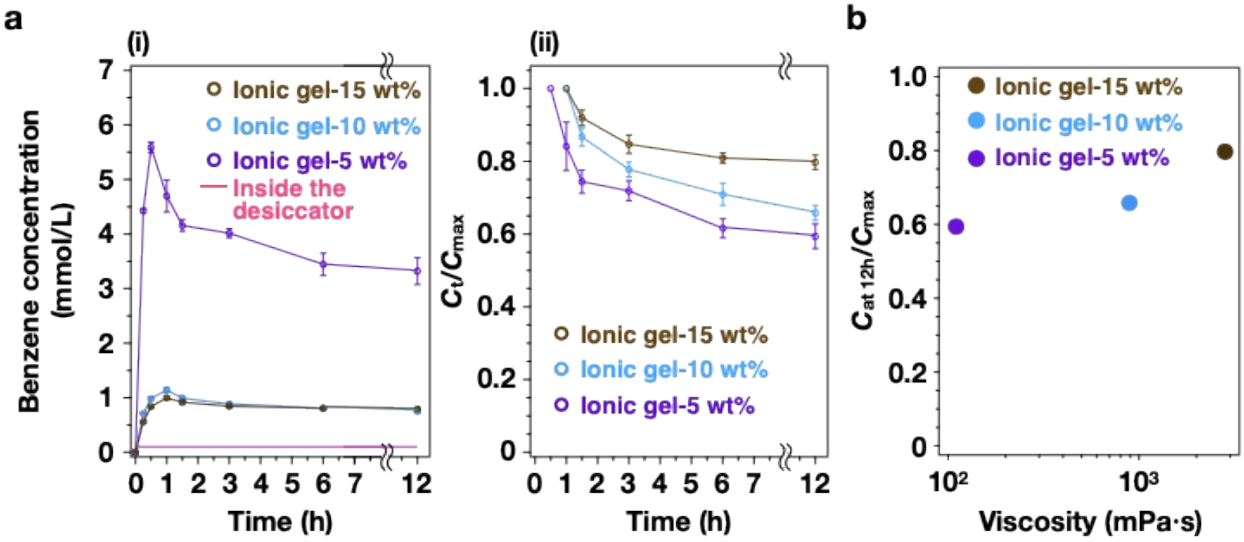

Supplementary Figure 12 | (a) (i) Benzene concentration and (ii) normalized concentration (C_t/C_{max}) as functions of time. The benzene concentration in the desiccator was 0.048 mmol/L. (b) Benzene retention efficiency as a function of viscosity over the experimental time range.

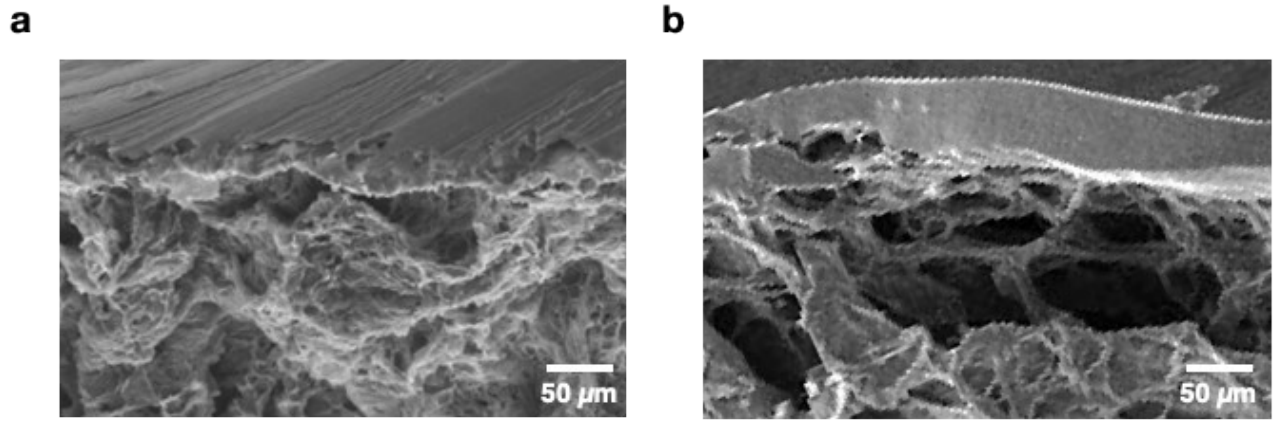

Supplementary Figure 13 | SEM images of the cross section of the ionic gels with a concentration of (a) 10 and (b) 15 wt% indicating a denser polymer layer at the interface.

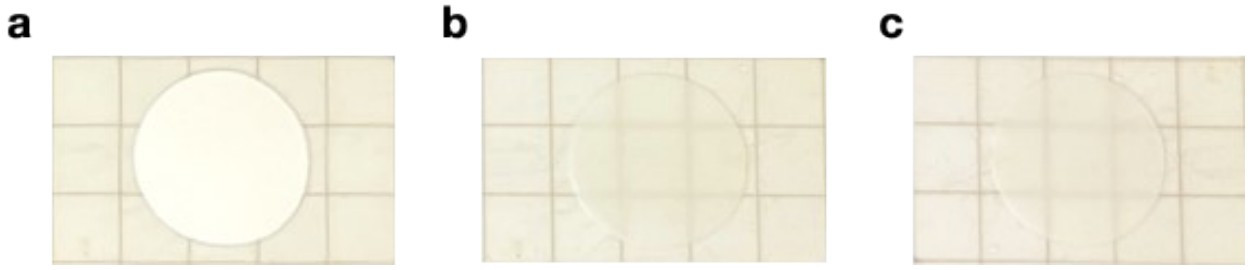

Supplementary Figure 14 | Photographs of (a) nylon membrane and nylon membrane coated with (b) DMSO and (c) 5 wt% ionic gel.

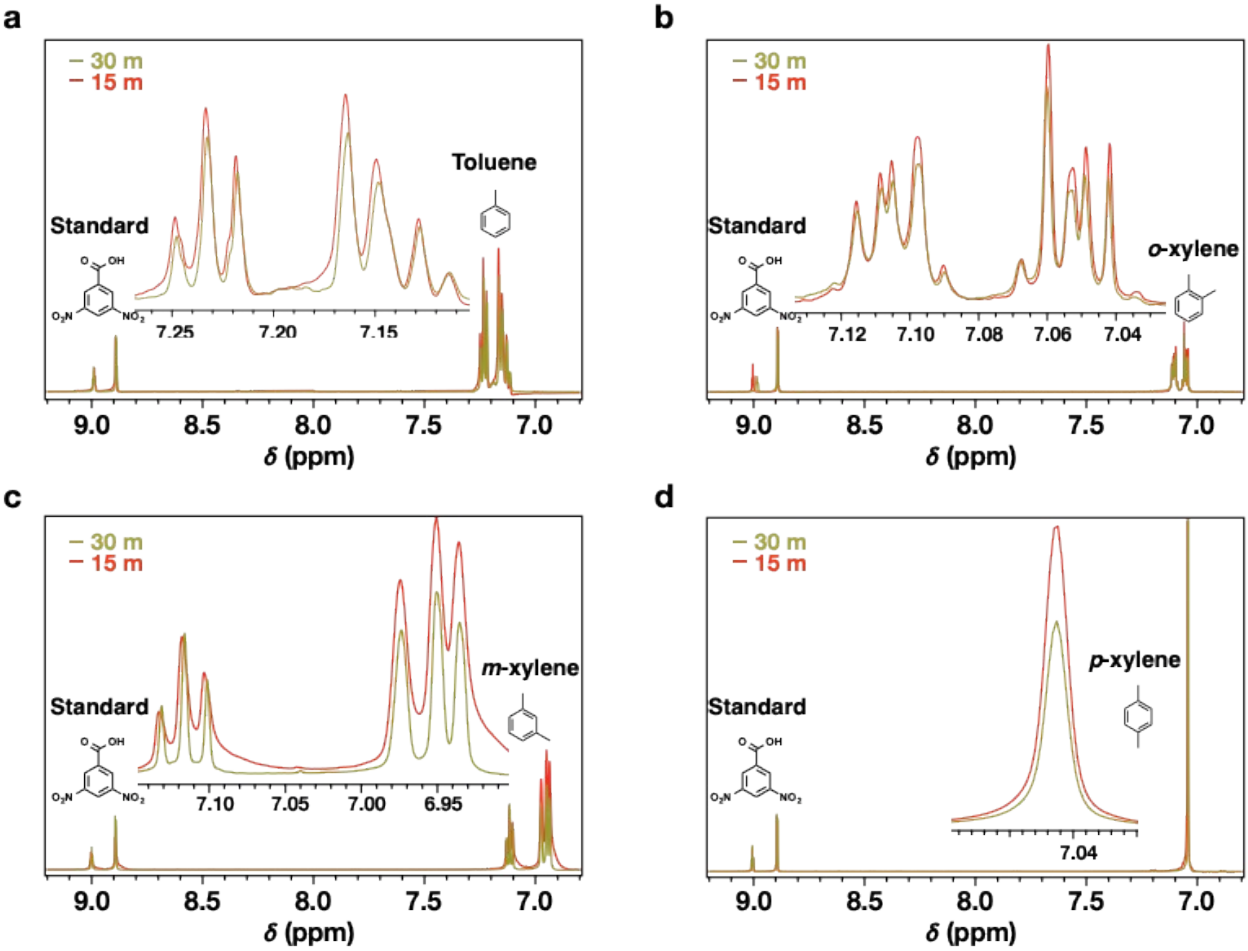

Supplementary Figure 15 | Concentration of (a) toluene, (b) *o*-xylene, (c) *m*-xylene, (d) *p*-xylene in DMSO that was measured over time in a closed system by ^{1}H NMR spectroscopy.

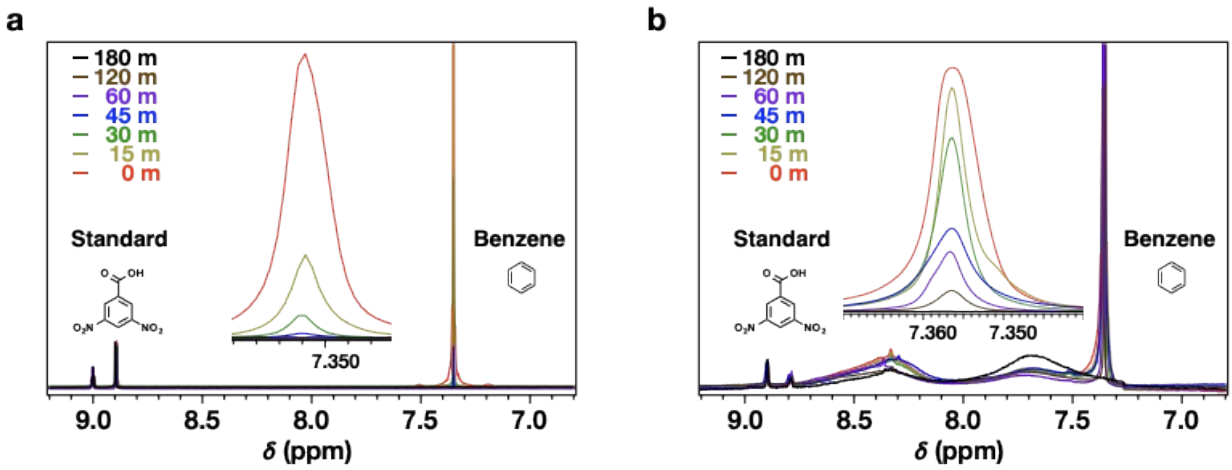

Supplementary Figure 16 | Concentration of benzene in (a) DMSO and (b) ionic gel measured over time in an open system by ^{1}H NMR spectroscopy.

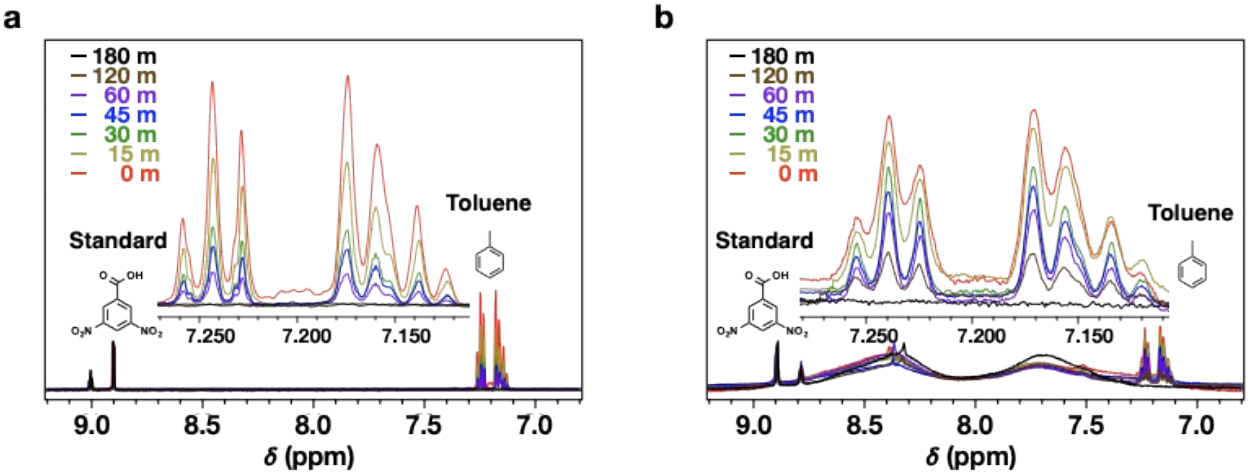

Supplementary Figure 17 | Concentration of toluene in (a) DMSO and (b) ionic gel measured over time in an open system by ^{1}H NMR spectroscopy.

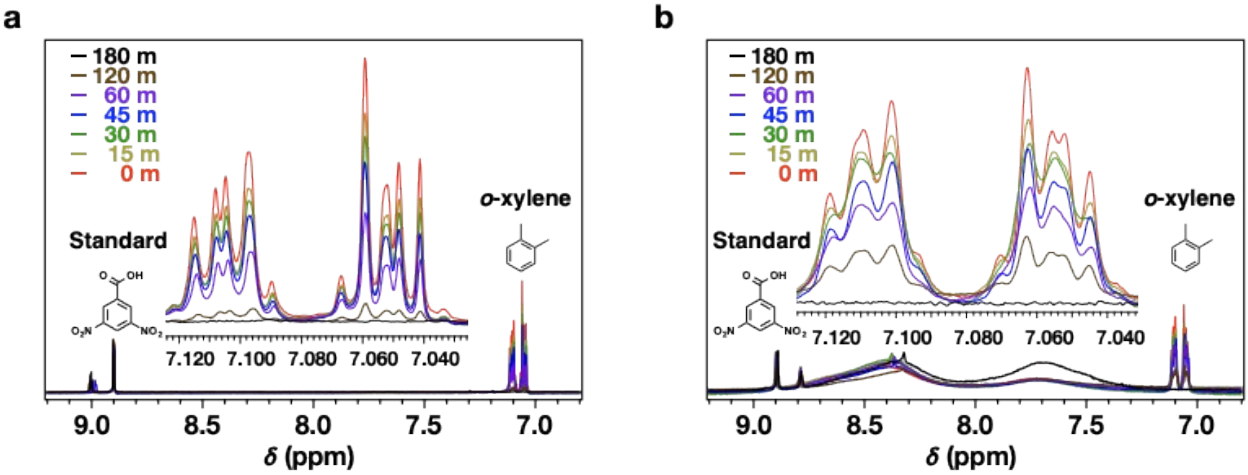

Supplementary Figure 18 | Concentration of *o*-xylene in (a) DMSO and (b) ionic gel measured over time in an open system by ^{1}H NMR spectroscopy.

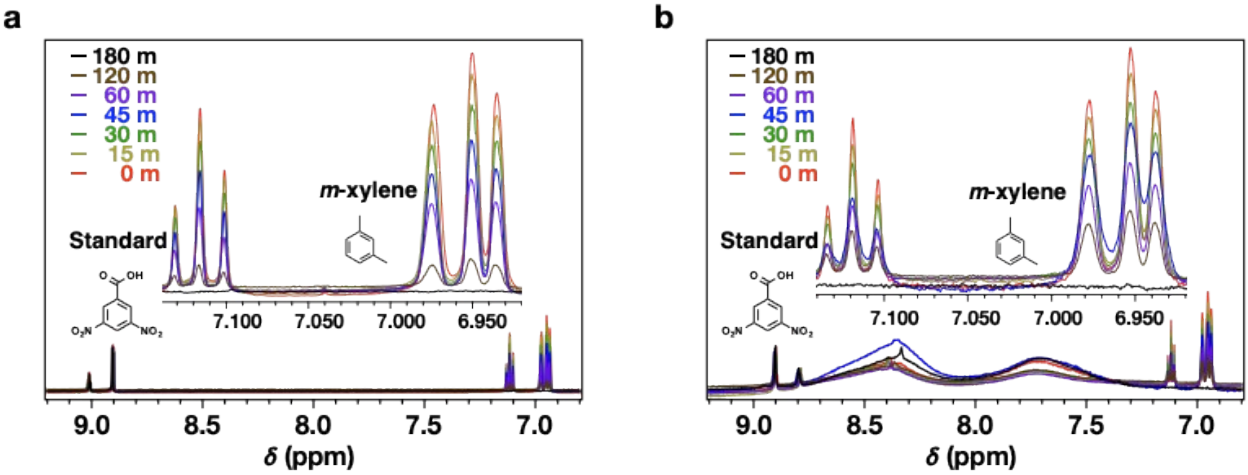

Supplementary Figure 19 | Concentration of *m*-xylene in (a) DMSO and (b) ionic gel measured over time in an open system by ^{1}H NMR spectroscopy.

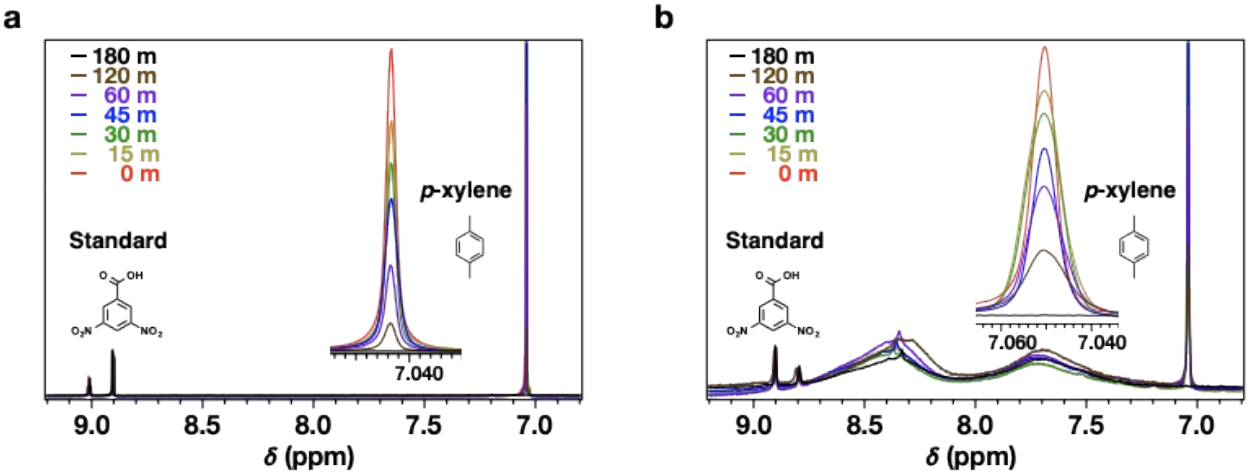

Supplementary Figure 20 | Concentration of *p*-xylene in (a) DMSO and (b) ionic gel measured over time in an open system by ^{1}H NMR spectroscopy.

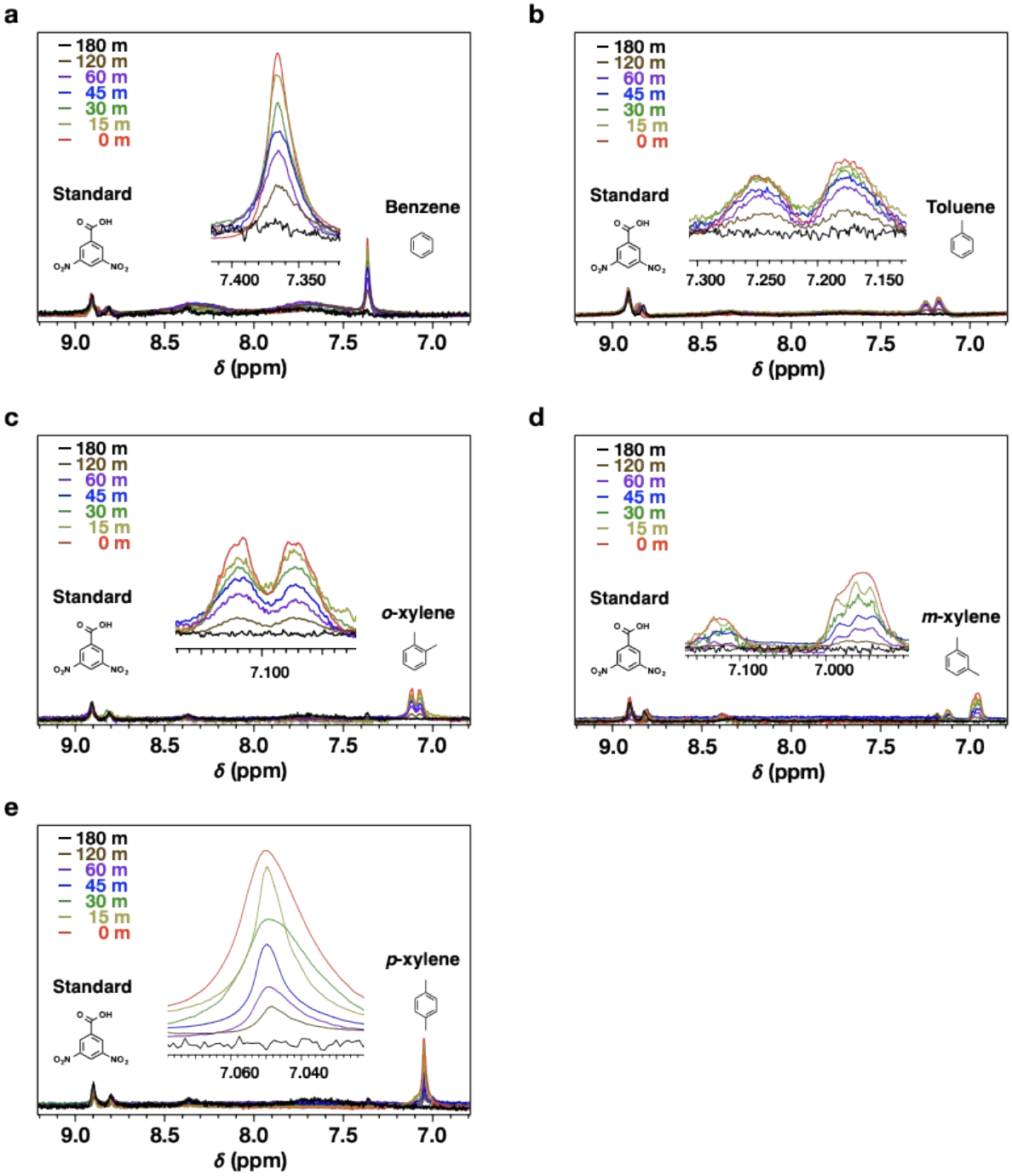

Supplementary Figure 21 | Concentrations of (a) benzene, (b) toluene, (c) *o*-xylene, (d) *m*-xylene, and (e) *p*-xylene in 15 wt% ionic gel measured over time in an open system through ^{1}H NMR spectroscopy.

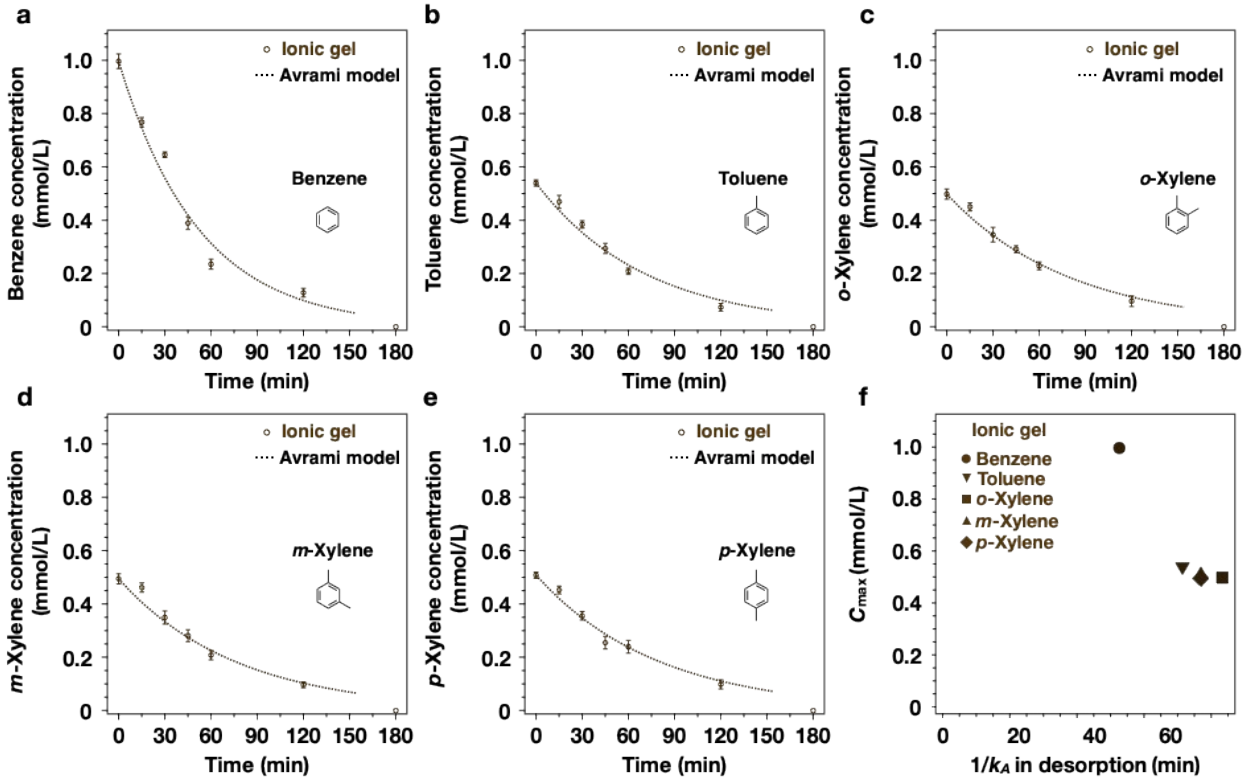

Supplementary Figure 22 | (a) Benzene, (b) toluene, (c) *o*-xylene, (d) *m*-xylene, and (e) *p*-xylene concentrations in 15 wt% ionic gel with respect to time in an open system. (f) Maximum absorption concentration (C_{max}) with respect to the reciprocal of the Avrami constant ($1/k_A$) in the desorption of the VOCs over the experimental time range.

9. Supplementary Tables 1–4

Supplementary Table 1 Monomer conversion and GPC characterization of P(DMA_{750}) via one-pot synthesis RAFT polymerization in a 10 mM phosphate buffer solution at 70 °C with a V-50 initiator.

Block	Polymer	Monomer conversion[a] (%)	$M_{n,GPC}$[b] (g mol^{-1})	$Đ$[b]
1	Poly(DMA_{750})	> 99	62,433	1.12

[a] Determined by ^{1}H NMR. [b] Determined using GPC.

Supplementary Table 2 Monomer conversion and GPC characterization of triblock P($AMPS_{150}$-*b*-DMA_{750}-*b*-$AMPS_{150}$) polyelectrolyte via one-pot synthesis RAFT polymerization in a 10 mM phosphate buffer solution at 70 °C with a V-50 initiator.

Block	Polymer	Monomer conversion[a] (%)	$M_{n,GPC}$[b] (g mol^{-1})	$Đ$[b]
1	Poly(DMA_{750})	> 99	62,433	1.12
2	Poly($AMPS_{150}$-*b*-DMA_{750})	99	78,220	1.18
3	Poly($AMPS_{150}$-*b*-DMA_{750}-*b*-$AMPS_{150}$)	99	94,749	1.24

[a] Determined by ^{1}H NMR. [b] Determined using GPC.

Supplementary Table 3 Monomer conversion and GPC characterization of triblock P($APTC_{150}$-*b*-DMA_{750}-*b*-$APTC_{150}$) polyelectrolyte via one-pot synthesis RAFT polymerization in a 10 mM phosphate buffer solution at 70 °C with a V-50 initiator.

Block	Polymer	Monomer conversion[a] (%)	$M_{n,GPC}$[b] (g mol^{-1})	$Đ$[b]
1	Poly($APTC_{150}$)	> 99	12,781	1.23
2	Poly($APTC_{150}$-*b*-DMA_{750})	99	52,676	1.30
3	Poly($APTC_{150}$-*b*-DMA_{750}-*b*-$APTC_{150}$)	99	68,216	1.43

[a] Determined by ^{1}H NMR. [b] Determined using GPC.

Supplementary Table 4 Avrami kinetic model parameters of 15 wt% ionic gel in the open system.

VOC	k_A (min^{-1})	R^2	$1/k_A$ (min)
	Ionic gel	Ionic gel	Ionic gel
Benzene	0.019	0.972	52.632
Toluene	0.014	0.978	71.429
o-Xylene	0.012	0.984	83.333
m-Xylene	0.013	0.981	76.923
p-Xylene	0.013	0.969	76.923

10. References

1 Q. Liu, J. Shi, S. Zheng, M. Tao, Y. He, and Y. Shi, *Ind. Eng. Chem. Res.*, 2014, 53, 11677–11683.

2 M. Deng and H. G. Park, *Langmuir*, 2019, 35, 4453–4459.

3 M. Avrami, *J. Chem. Phys.*, 1941, 9, 177–184.